Nucleic Acids Research, 1997, Vol. 25, No. 21 **4379–4384**

Phase imaging of moving DNA molecules and DNA molecules replicated in the atomic force microscope

Miriam Argaman, Roxana Golan, Neil H. Thomson and Helen G. Hansma*

Department of Physics, University of California, Santa Barbara, CA 93106, USA

Received June 9, 1997; Revised and Accepted September 12, 1997

ABSTRACT

Phase imaging with a tapping mode atomic force microscope (AFM) has many advantages for imaging moving DNA and DNA–enzyme complexes in aqueous buffers at molecular resolution. In phase images molecules can be resolved at higher scan rates and lower forces than in height images from the AFM. Higher scan rates make it possible to image faster processes. At lower forces the molecules are imaged more gently. Moving DNA molecules are also resolved more clearly in phase images than in height images. Phase images in tapping mode AFM show the phase difference between oscillation of the piezoelectric crystal that drives the cantilever and oscillation of the cantilever as it interacts with the sample surface. Phase images presented here show moving DNA molecules that have been replicated with Sequenase in the AFM and DNA molecules tethered in complexes with *Escherichia coli* RNA polymerase.

INTRODUCTION

The atomic force microscope (AFM) can image DNA molecules and DNA–enzyme interactions in aqueous buffers at a resolution of ~3–10 nm (1–3). It is relatively easy to observe the progressive degradation of individual DNA molecules by non-specific nucleases such as DNase I (4) and *Bal*31 (5) by atomic force microscopy (AFM). It is also possible to observe non-specific binding of *Escherichia coli* RNA polymerase (RNAP) to DNA that has been previously dried onto a mica surface (6).

With difficulty it is possible to observe the progress of active RNAP moving along a DNA template during transcription in a tapping mode AFM (7,8). The reason for this difficulty is that the DNA must be free to move through the RNAP for transcription to occur, but the DNA must be bound reasonably well to the mica surface for good AFM imaging. Moving DNA molecules can be imaged by AFM (3,4,9–11). However, in most experiments the DNA is either bound to the mica too tightly to move or is moving too freely to be seen clearly in height images with the AFM. We have found that moving DNA molecules can often be visualized much more clearly in the AFM in phase images than in height images.

Phase images are a new type of AFM image that can be obtained with tapping mode AFM. Phase images show the phase difference between oscillation of the piezoelectric crystal that drives the cantilever and oscillation of the cantilever as it interacts with the sample surface (Fig. 1; 12).

Phase imaging with the AFM has previously been shown to be useful for samples in air, where it can be used to identify features on the sample surface that are not easily distinguished by height (13–15). Here we show that phase imaging is also useful in aqueous buffers for samples such as DNA and DNA–enzyme complexes.

MATERIALS AND METHODS

Ruby mica (S and J Trading Co., Glen Oaks, NY) was freshly cleaved with tape prior to use. Ni-treated mica was prepared by pipetting 5 µl 1 mM $NiCl_2$ onto freshly cleaved mica, rinsing after 1 min with MilliQ water (Millipore, Burlington, MA) and drying with compressed air (9).

PCR of the 967 bp DNA

A 967 bp DNA derived from $pTZtR_2$ (16) was prepared with two oligos: 5′-ACTATAGGGAAAGCTTGCATGCCTG-3′ (201 reverse oligo) and 5′-AAAAAAGGGAATAAGGGCGACACGG-3′ (2234-1KB). The reaction was carried out in a volume of 100 µl of 1× Taq polymerase transcription buffer, 20 ng $pTZtR_2$ plasmid, 10 pmol each oligo and dNTPs (Pharmacia, Piscataway, NJ) to a final concentration of 250 pmol/µl. The DNA was amplified in 30 cycles of 1 min 94°C, 1 min 52°C, 1.5 min 70°C and a final cycle of 1 min 94°C, 1 min 52°C and 8 min 70°C. The 967 bp PCR fragment was purified from the reaction mixture using a PCR product purification kit (Jet Pure; Genomed Inc., Research Triangle Park, NC). This 967 bp DNA, used as a template for the RNAP complexes, has a T7A1 promoter and a tR_2 terminator (16). The $pTZTR_2$ plasmid was provided by M.Kashlev.

Priming of ϕX-174 virion DNA

Aliquots of 15 µg ϕX-174 virion DNA (US Biochemical, Cleveland, OH) were incubated with 100 pmol ϕX primer in a total volume of 50 µl. The priming mixture was heated to 65°C for 2 min and gradually cooled to 2°C. The sequence of the ϕX-174 primer was 5′-TCATGGAAGCGATAAAACTC-3′ (provided by R.L.Sinsheimer).

Sample preparation

RNAP–DNA complexes. Stalled ternary complexes of *E.coli* RNAP (US Biochemical) and the 967 bp DNA were made as

*To whom correspondence should be addressed. Tel: +1 805 893 3881; Fax: +1 805 893 8315; Email: hhansma@physics.ucsb.edu

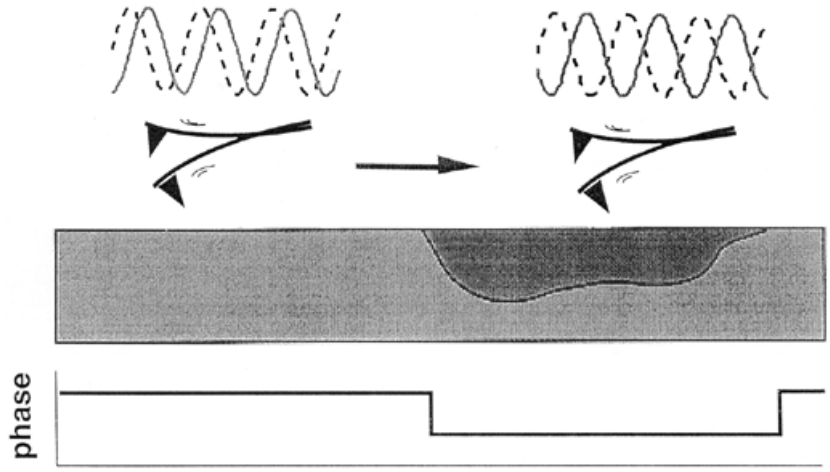

Figure 1. Diagram of phase imaging with the tapping mode AFM. Phase imaging measures the phase lag of the cantilever oscillation (solid wave) relative to the piezo drive (dashed wave). Spatial variations in sample properties cause shifts in the phase of the two waves, which are mapped to produce phase images. From ref. 12.

described for a 373 bp DNA (7). Complexes were then diluted 1:40 to a final concentration of ~1 ng DNA/µl. An aliquot of 7 µl was pipetted onto freshly split mica and inserted into the AFM without drying. Buffer was flowed into the fluid cell using a gravity-driven flow system (17). Imaging was carried out in the buffers specified in the figure captions.

Plasmid DNA. Plasmid Bluescript II SK^+ (Stratagene, La Jolla, CA) was diluted into 5 mM HEPES, 5 mM KCl and 2 mM $MgCl_2$ to a final concentration of 1 ng/µl. Aliquots of 30 µl DNA solution were pipetted onto the AFM fluid cell. The fluid cell was inserted into the AFM over Ni-treated mica.

ϕX-174 RF DNA Hinc*II digest.* The ϕX-174 RF DNA *Hinc*II digest (Pharmacia, Piscataway, NJ) was diluted into 10 mM HEPES, 1 mM $CoCl_2$ to a final concentration of 2.5 ng/µl. Aliquots of 30 µl were loaded onto the AFM fluid cell and inserted into the AFM over freshly split mica.

Replication of ϕX-174 viron DNA. A reaction mixture was prepared containing 0.7 ng/µl primed ϕX-174 virion DNA and 600 µM dNTPs in a MOPS-Mn buffer (40 mM MOPS, pH 7.4, 10 mM $MgCl_2$, 50 mM NaCl, 5 mM $MnCl_2$). A fluid cell with an O-ring was inserted into the AFM over Ni-treated mica. The MOPS-Mn buffer was injected into the fluid cell. Once conditions for imaging were adjusted with the buffer alone, 0.8 U Sequenase enzyme (US Biochemical) were added to the reaction mixture and the reaction mixture was injected into the AFM and imaged.

AFM imaging

Tapping mode AFM in fluid was carried out using a MultiMode AFM with a phase base and a Nanoscope III with extender electronics (Digital Instruments, Santa Barbara, CA). Silicon nitride cantilevers, 100 µm long with narrow arms (Digital Instruments), were inserted into a Plexiglas fluid cell. Electron beam deposition (EBD) tips were grown onto the silicon nitride cantilevers. Some of the EBD tips were sharpened by glow discharge (18). Images were acquired simultaneously with the height and phase signals.

Prior to imaging the phase signal was adjusted to zero using the 'zero phase' command. Imaging forces were increased and decreased by lowering and raising the set point.

Tip speeds were calculated from the scan rates and the scan sizes. For a scan size of 1×1 µm the tip speed in µm/s is twice the scan rate in Hz, because the scan rate is the number of cycles/s that the tip scans back and forth across the sample.

Description of the phase, amplitude and height signals

In tapping mode AFM a tip on the end of an oscillating cantilever briefly touches the surface during each oscillation as it scans the sample (Fig. 1; 19–21). The cantilever is driven by an oscillating piezoelectric transducer that provides a driving force of constant amplitude and frequency. When tapping in fluid many resonances (peaks) appear in the spectrum of the response of the cantilever (amplitude versus piezo drive frequency) that do not necessarily correspond to the cantilever's resonance (22,23). The oscillation frequency in these experiments, ~13 kHz, was a peak near the thermal resonance of the cantilever but of high enough frequency to be inaudible.

The motion of the cantilever is monitored by bouncing a laser beam off its back surface onto a split photodiode. The AFM generates signals representing dynamic motion of the cantilever: its amplitude and phase. The amplitude is the magnitude of the cantilever's response to the driving force and decreases when the cantilever touches the surface. A feedback loop adjusts the height of the sample through a piezoelectric transducer to keep the amplitude at its set point. The height changes in the sample form the height image, representing the topography of the sample. The phase signal measures the time lag between the piezo drive and the actual motion of the cantilever. The changes in the phase lag of the cantilever motion form the phase image.

RESULTS

Imaging with a faster scan rate

As the scan rate is increased the quality of AFM image gradually deteriorates. The phase image remains clear, however, at scan rates where the height image in tapping mode contains very little

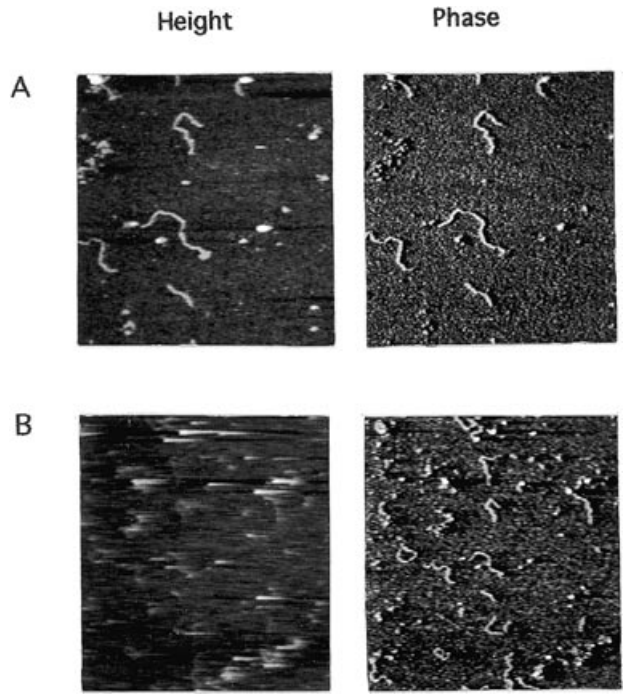

Figure 2. Effect of scan rate on height and phase images with tapping mode AFM. Simultaneously acquired height and phase images are of DNA deposited onto freshly split mica in a complex with RNAP and imaged in Zn buffer (20 mM Tris, 5 mM $MgCl_2$, 50 mM KCl, 1 mM β-mercaptoethanol, 2 mM $ZnCl_2$, pH 7.9). An EBD tip was used. (**A**) Scan rate 9.2 Hz (tip speed 18.4 Hz), image size 1 × 1 µm. (**B**) Scan rate 27.5 Hz (tip speed 110 Hz), image size 2 × 2 µm.

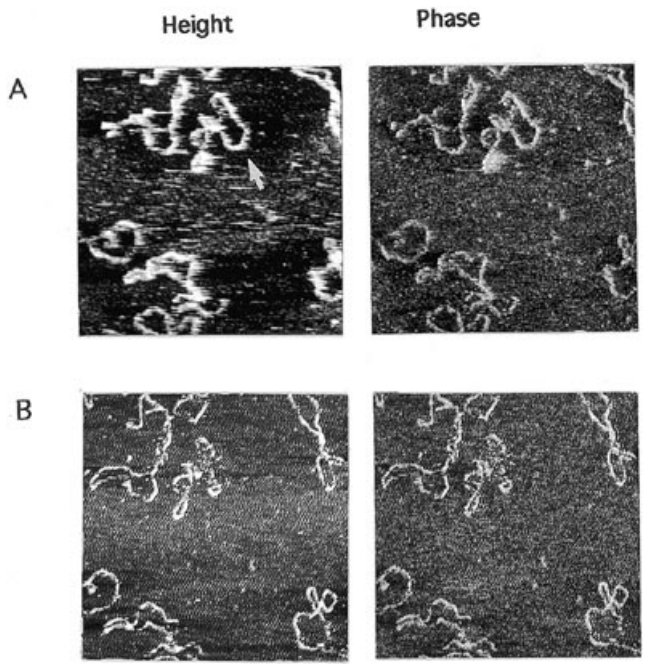

Figure 3. Effect of imaging force on height and phase images with tapping mode AFM. Simultaneously acquired phase and height images are of plasmid Bluescript on Ni^{2+}-coated mica in a 5 mM HEPES, 5 mM KCl and 2 mM $MgCl_2$ buffer. Images in (**A**) were acquired at a lower force than images in (**B**). The set point was lowered 6% between (A) and (B). The arrow in (A) shows a loop of DNA that has moved in (B). The sample was scanned with an EBD tip. Scan rate 6.1 Hz, scan size 1 × 1 µm.

information (Fig. 2). The DNA in these images was in a buffer supplemented with Zn^{2+}, which enables one to obtain stable images of DNA without intermediate drying (11,17). At a scan rate of 9.16 Hz (lines/s) the DNA was seen clearly in both height and phase images (Fig. 2A). When the scan rate was raised to 27.5 Hz the height image became blurred, while the phase image remained clear (Fig. 2B). When the scan rate was increased further the phase image also became blurred.

It is advantageous to be able to image at a high scan rate, because the interval between successive images is shorter, which enables one to image biological processes with a higher time resolution.

Imaging with lower forces

As the imaging force is reduced, the height image becomes blurry at reduced forces where the phase image is still sharp (Fig. 3A). At a higher imaging force both height and phase images are sharp (Fig. 3B). For non-destructive imaging of biological samples it is advantageous to use the lowest possible imaging forces.

One of the plasmid DNA molecules in Figure 3 is moving on the mica surface (arrow). It has a loop that has either moved between the two images or has been dislodged by the AFM tip in the higher force scans of Figure 3B.

The DNA molecules in Figure 4 are also moving, because this image was taken soon after DNA in buffer was pipetted onto the Plexiglas fluid cell, which was then mounted in the AFM above Ni-treated mica. This DNA is a *Hin*cII digest of ϕX-174 DNA, which contains DNA molecules of ~ 25–350 nm in length. Again,

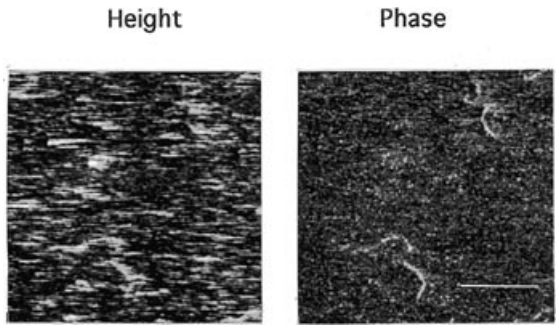

Figure 4. Simultaneously acquired height and phase images of settling DNA in a buffer containing 10 mM HEPES, 1 mM $CoCl_2$, pH 7.0, acquired by tapping mode AFM. The DNA molecules are a *Hin*cII digest of ϕX-174 DNA. Scan rate 4.7 Hz. Scale bar 300 nm.

the DNA molecules can be seen more clearly in phase than in height images. In an image taken 5 min later, at approximately the same imaging force, the DNA molecules were also clearly visible in the height image (data not shown). This is consistent with our earlier observations that DNA appears to bind more weakly to mica in the first 5 min after application to the mica (11).

Phase images are often a useful adjunct to height images, because they can help confirm the existence and/or conformation of features on the sample surface, such as DNA. Thus, phase images often serve as a sort of 'second opinion' for height images. For example, it appears that there may be a DNA molecule in the

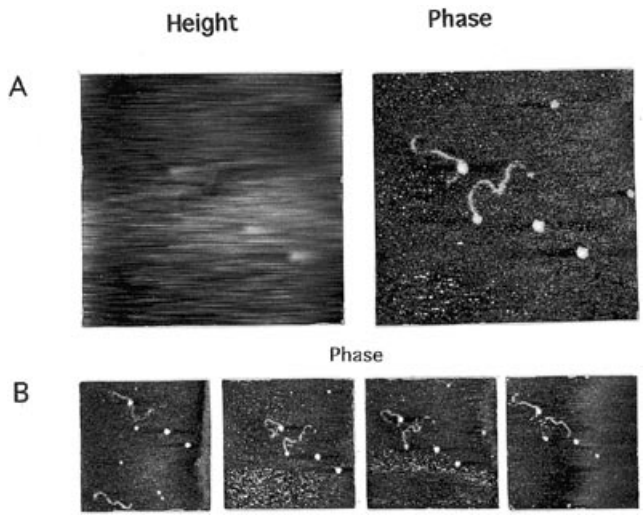

Figure 5. (**A**). Simultaneously acquired height and phase images of RNA polymerase–DNA complexes imaged in Co buffer (20 mM Tris, 4 mM $MgCl_2$, 50 mM KCl, 6 mM $CoCl_2$, pH 7.0, and 10 μM NTPs) with a sharpened EBD tip. (**B**) Phase images taken, from left to right respectively, 4, 14, 18 and 20 min after addition of NTPs to the flowing buffer. The tethered DNA molecules are moving freely in the buffer and are imaged by tapping mode AFM. Scan rate 6.1 Hz, scan size 1 × 1 μm for all images.

lower part of the height image in Figure 4. The presence of this DNA molecule is confirmed in the phase image of Figure 4.

Phase images are also improved by imaging at lower gains. Lower gains correspond to a slower response of the electronic feedback to sample surface features.

Imaging DNA in complexes with RNAP

RNAP–DNA complexes were imaged with a buffer containing Co^{2+}, because Co^{2+}, as well as Ni^{2+} and Zn^{2+}, are useful for imaging loosely bound DNA in fluid in the AFM (11). This Co^{2+} buffer could support transcription in a test tube as seen by AFM in air with a rolling circle DNA template (24; Hansma *et al*., in preparation).

The RNAP–DNA complexes in Figure 5 were scanned in tapping mode AFM with a sharpened EBD tip, using a flow system to change buffers during imaging (17). RNAP–DNA complexes and uncomplexed RNAP molecules were clearly visualized in the phase images of Figure 5, while even the RNAP molecules were barely seen in the height images. The DNA molecules were quite mobile, as can be seen in the sequence of four phase images in Figure 5B. The simultaneously acquired height images were as blurry as the height image in Figure 5A and are not shown.

In the series of images in Figure 5B the two RNAP–DNA complexes are seen with the tethered DNA molecules moving rather freely in the buffer. Attempts to improve the height images were unsuccessful. The differences between the images acquired with the height and phase signals are not necessarily due to the use of a sharpened tip, because such differences were sometimes seen with a non-sharpened EBD tip as well.

Replication of ϕX-174 viron DNA in the AFM

Successive stages in DNA replication were imaged by AFM of a reaction mixture that was pipetted onto the fluid cell at $t = 0$ min after the enzyme was added to the reaction mixture. AFM images captured during the first 20 min showed only ssDNA (Fig. 6A). The single-stranded molecules of ϕX-174 DNA were folded into star-like structures due to intermolecular base pairing, as has been observed previously by AFM (9). At $t = 20$–60 min, strands of dsDNA ~300–600 bp long were seen in nearby areas (Fig. 6B). These lengths correspond to 5–11% replication of the ϕX-174 DNA molecules. At $t = 80$–90 min the longest dsDNA molecule was seen, in a different location on the mica surface (Fig. 6C). This long DNA molecule was tethered to the mica and its ends moved (Fig. 6D). The length of this molecule was ~4600 bp, corresponding to 85% replication. The replicated DNA molecules are seen more clearly in the phase images than in the height images.

For this experiment the mica was pre-treated with Ni^{2+}, which has been shown to improve the imaging of moving DNA molecules in the AFM (4,25). The Ni^{2+} may have inhibited the Sequenase somewhat, since 50% inhibition of Sequenase has been reported for 70 μM Ni^{2+} (26).

In this experiment the replicated dsDNA molecules are all linear. The ssDNA template from the ϕX-174 virion is circular, however, and in other experiments we have seen loops of dsDNA formed in the AFM and imaged under propanol (27). It appears that the replicated DNA molecules were nicked in this experiment.

At present we have been able to image DNA replicated in the AFM only when all components of the reaction mixture are combined outside the AFM and are placed immediately (at 't = 0') into the AFM. In these experiments the DNA may have replicated in solution in the AFM before binding to the mica. We are currently working toward our goal of imaging stages in the replication of individual DNA molecules on mica, but this is proving to be a challenge.

DISCUSSION

We have found that phase imaging broadens the range of conditions for useful AFM imaging in aqueous buffers and increases the amount of information obtained.

Phase imaging is optimal at lower imaging forces than height imaging (Fig. 3). This is a significant advantage for phase imaging over height imaging, since there is less damage to biological samples at lower imaging forces. In addition, phase images remained clear at a 3- to 6-fold faster scan rate than height images, 27.5 Hz in these experiments (Fig. 2), corresponding to a tip speed of 110 μm/s. With faster scan rates images can be captured more quickly for observing processes in the AFM.

In some experiments good data can be obtained only with phase imaging, because the height images are poor, for unknown reasons. The high quality phase images in Figure 5 show the movement of DNA molecules that cannot be detected in height images. In addition, phase imaging appears to be less sensitive to changes in the flow rate of buffer into the fluid cell or to external vibration.

Another use for phase imaging is that, in combination with height imaging, it gives a 'second opinion' about obscure features in the sample. For example, the series of images in Figure 6 shows that the newly replicated dsDNA was moving in the buffer. Although the

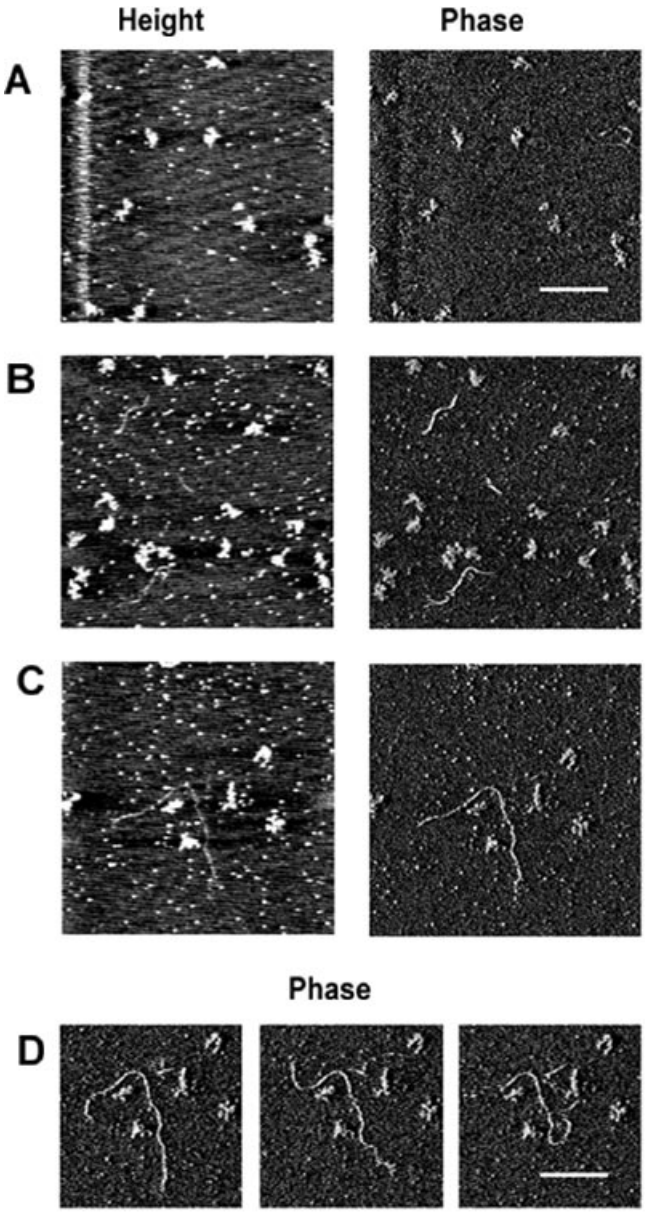

Figure 6. DNA replication in the AFM. Simultaneously acquired height and phase images show replication of ϕX-174 viron DNA (star-like molecules) into dsDNA (long molecules). (**A**) A field of ssDNA molecules. (**B**) Another field in the same sample with partly replicated ϕX-174 viron DNA. (**C**) An almost fully replicated ϕX-174 DNA molecule. (**D**) Three more images of the molecule shown in (C). The arms of this newly replicated DNA molecule are moving rather freely in the buffer. The sample was scanned by tapping mode AFM with an EBD tip. Scan rates 6.1 (A–C) and 12.2 Hz (D), image sizes 2 × 2 μm (A–C) and 1.3 × 1.3 μm (D). Scale bars 500 nm.

height image in Figure 6C is reasonably good, the contours of the dsDNA can be traced more reliably in the phase image.

Phase imaging requires not only a tapping AFM but also a phase base for the AFM and extra electronics. Amplitude imaging can be done with all tapping AFMs and has some of the same advantages as phase imaging. We have not experimented systematically with the amplitude images of moving DNA, but those who can do amplitude imaging but not phase imaging might find that amplitude imaging is also useful for imaging moving DNA at faster scan speeds and lower forces.

Phase imaging in air is sometimes better than height imaging for seeing low features such as DNA in large scans of 3–4 μm or more. In height images of large scan sizes, low features such as DNA are often hard to see because the sample surface appears to be lightly bowed or warped, so that height changes over the sample surface are larger than the height of the DNA. Since phase images detect changes in height instead of absolute height, one can sometimes see DNA molecules in phase images at scan sizes that are too large to see DNA molecules in height images.

The interpretation of phase images captured in air is currently being investigated. With some samples, such as polyethylene partially covering mica, phase shifts correlate with differences in stiffness (Young's modulus) of the different materials (14). With other samples, phase shifts correlate with adhesion (28). Differences in hydration may also affect phase shifts, with less hydrated regions appearing lighter and more hydrated regions appearing darker in phase images (15). Phase images in air appear very different at different imaging forces, because the tip–sample contact area is larger at higher imaging forces (14).

Phase images in aqueous buffers also appear different at different imaging forces. At high imaging forces phase images in aqueous buffers sometimes show little contrast and are therefore less useful than height images. Height images give information about the heights of features on the sample surface. Phase images do not give information about heights and are thus not a substitute for height images. We routinely capture simultaneous height and phase images in order to maximize the amount of information obtained during imaging.

Here we show images of long moving DNA molecules that were replicated in the AFM. Before the advent of phase imaging we were able to image DNA replicated in the AFM only after propanol was injected into the fluid cell (27), which immobilized the DNA (29). With more experience we hope to be able to follow enzymatic processes such as DNA replication in the AFM more clearly with phase imaging.

As AFM development continues, the AFM is becoming increasingly useful for research on DNA and other biomaterials (30–32). One way in which AFM development is continuing is that new types of imaging are being introduced. One of these types of imaging is phase imaging. We have shown here that phase imaging in aqueous buffers is particularly useful for AFM of moving DNA molecules and DNA–enzyme complexes.

ACKNOWLEDGEMENTS

We thank Tilman Schäffer for critically reading the manuscript, Bettye Smith for helpful discussions, Scott Hansma for software development, Daniel Laney for making the Plexiglas fluid cells and Christine Chen for expert technical assistance. This work was supported by NSF MCB9604566 (M.A., H.H. and R.G.), NSF DMR9632716 (M.A.) and NSF DMR9622169 (N.T.).

REFERENCES

1 Mou,J., Czajkowsky,D.M., Zhang,Y. and Shao,Z. (1995) *FEBS Lett.*, **371**, 279–282.
2 Hansma,H.G., Bezanilla,M., Zenhausern,F., Adrian,M. and Sinsheimer,R.L. (1993) *Nucleic Acids Res.*, **21**, 505–512.
3 Lyubchenko,Y.L. and Shlyakhtenko,L.S. (1997) *Proc. Natl. Acad. Sci. USA*, **94**, 496–501.

4 Bezanilla,M., Drake,B., Nudler,E., Kashlev,M., Hansma,P.K. and Hansma,H.G. (1994) *Biophys. J.*, **67**, 2454–2459.
5 Bustamante,C., Erie,D.A. and Keller,D. (1994) *Curr. Opin. Struct. Biol.*, **4**, 750–760.
6 Guthold,M., Bezanilla,M., Jenkins,B., Hansma,H. and Bustamante,C. (1994) *Proc. Natl. Acad. Sci. USA*, **91**, 12927–12931.
7 Kasas,S., Thomson,N.H., Smith,B.L., Hansma,H.G., Zhu,X., Guthold,M., Bustamante,C., Kool,E.T., Kashlev,M. and Hansma,P.K. (1997) *Biochemistry*, **36**, 461–468.
8 Guthold,M., Zhu,X., Rivetti,C., Yang,G., Thomson,N.H., Kasas,S., Smith,B., Hansma,H.G., Hansma,P.K. and Bustamante,C. (1997) submitted.
9 Hansma,H.G., Bezanilla,M., Laney,D.L., Sinsheimer,R.L. and Hansma,P.K. (1995) *Biophys. J.*, **68**, 1672–1677.
10 Hansma,H.G., Laney,D.E., Revenko,I., Kim,K. and Cleveland,J.P. (1996) In Sarma,R.H. and Sarma,M.H. (eds), *Biological Structure and Dynamics*. Adenine Press, Albany, NY, Vol. 2, pp. 249–258.
11 Hansma,H.G. and Laney,D.E. (1996) *Biophys. J.*, **70**, 1933–1939.
12 Babcock,K.L. and Prater,C.B. (1995) Digital Instruments, Santa Barbara, CA.
13 Magonov,S.N., Elings,V. and Papkov,V.S. (1996) *Polymer*, **38**, 297–307.
14 Magonov,S.N., Elings,V. and Whangbo,M.-H. (1997) *Surface Sci. Lett.*, **375**, L385–L391.
15 Hansma,H.G., Kim,K.J., Laney,D.E., Garcia,R.A., Argaman,M. and Parsons,S.M. (1997) *J. Struct. Biol.*, **119**, 99–108.
16 Kashlev,M., Martin,E., Polyakov,A., Severinov,K., Nikiforov,V. and Goldfarb,A. (1993) *Gene*, **130**, 9–14.
17 Thomson,N.H., Kasas,S., Smith,B., Hansma,H.G. and Hansma,P.K. (1996) *Langmuir*, **12**, 5905–5908.
18 Wendel,M., Lorenz,H. and Kotthaus,J.P. (1995) *Appl. Phys. Lett.*, **67**, 3732–3734.
19 Burnham,N.A., Behrend,O.P., Oulevey,F., Gremaud,G., Gallo,P.-J., Gourdon,D., Dupas,E., Kulik,A.J., Pollock,H.M. and Briggs,G.A.D. (1997) *Nanotechnol.*, **8**, 67–75.
20 Hansma,H.G., Sinsheimer,R.L., Groppe,J., Bruice,T.C., Elings,V., Gurley,G., Bezanilla,M., Mastrangelo,I.A., Hough,P.V.C. and Hansma,P.K. (1993) *Scanning*, **15**, 296–299.
21 Zhong,Q., Inniss,D., Kjoller,K. and Elings,V.B. (1993) *Surface Sci. Lett.*, **290**, L888–L692.
22 Putman,C.A.J., van der Werf,K.O., deGrooth,B.G. and van Hulst,N.F. (1994) *Appl. Phys. Lett.*, **64**, 2454.
23 Schäffer,T.E., Cleveland,J.P., Ohnesorge,F., Walters,D.A. and Hansma,P.K. (1996) *J. Appl. Phys.*, **80**, 3622–3627.
24 Daubendiek,S.L., Ryan,K. and Kool,E.T. (1995) *J. Am. Chem. Soc.*, **117**, 7818–7819.
25 Hansma,H.G., Browne,K.A., Bezanilla,M. and Bruice,T.C. (1994) *Biochemistry*, **33**, 8436–8441.
26 Snow,E.T., Xu,L. and Kinney,P.L. (1993) *Chemico-Biol. Interact.*, **88**, 155–173.
27 Hansma,H.G. (1996) *J. Vacuum Sci. Technol. B*, **14**, 1390–1394.
28 vanNoort,S.J.T., van der Werf,K.O., de Grooth,B.G., van Hulst,N.F. and Greve,J. (1997) *Ultramicroscopy*, in press.
29 Hansma,H.G., Vesenka,J., Siegerist,C., Kelderman,G., Morrett,H., Sinsheimer,R.L., Bustamante,C., Elings,V. and Hansma,P.K. (1992) *Science*, **256**, 1180–1184.
30 Hansma,H.G. and Hoh,J. (1994) *Annu. Rev. Biophys. Biomol. Struct.*, **23**, 115–139.
31 Shao,Z., Mou,J., Czaijkowsky,D.M., Yang,J. and Yuan,J.-Y. (1996) *Adv. Phys.*, **45**, 1–86.
32 Bustamante,C. and Rivetti,C. (1996) *Annu. Rev. Biophys. Biomol. Struct.*, **25**, 395–429.